# Molecular Dynamics in Living Cells Observed by Fluorescence Correlation Spectroscopy with One- and Two-Photon Excitation

Petra Schwille, Ulrich Haupts, Sudipta Maiti, and Watt W. Webb
School of Applied and Engineering Physics, Cornell University, Ithaca, New York 14853 USA

ABSTRACT Multiphoton excitation (MPE) of fluorescent probes has become an attractive alternative in biological applications of laser scanning microscopy because many problems encountered in spectroscopic measurements of living tissue such as light scattering, autofluorescence, and photodamage can be reduced. The present study investigates the characteristics of two-photon excitation (2PE) in comparison with confocal one-photon excitation (1PE) for intracellular applications of fluorescence correlation spectroscopy (FCS). FCS is an attractive method of measuring molecular concentrations, mobility parameters, chemical kinetics, and fluorescence photophysics. Several FCS applications in mammalian and plant cells are outlined, to illustrate the capabilities of both 1PE and 2PE. Photophysical properties of fluorophores required for quantitative FCS in tissues are analyzed. Measurements in live cells and on cell membranes are feasible with reasonable signal-to-noise ratios, even with fluorophore concentrations as low as the single-molecule level in the sampling volume. Molecular mobilities can be measured over a wide range of characteristic time constants from $\sim 10^{-3}$ to $10^{3}$ ms. While both excitation alternatives work well for intracellular FCS in thin preparations, 2PE can substantially improve signal quality in turbid preparations like plant cells and deep cell layers in tissue. At comparable signal levels, 2PE minimizes photobleaching in spatially restrictive cellular compartments, thereby preserving long-term signal acquisition.

## INTRODUCTION

Derived and first applied to measure diffusion and chemical kinetics of DNA-drug intercalation (Magde et al., 1972, 1974; Elson and Magde), fluorescence correlation spectroscopy (FCS) has recently experienced growing popularity in biochemical and biophysical applications due to significantly improved signal-to-background ratios and single-molecule sensitivity (Rigler and Widengren, 1990; Mets and Rigler, 1994). Thus dynamic studies of minute amounts of freely diffusing, biochemically active molecules and particles, including nucleic acids (Kinjo and Rigler, 1995; Schwille et al., 1996) and proteins (Rauer et al., 1996; Bieschke and Schwille, 1997), in time ranges from microseconds to seconds became readily practicable. The analytical and diagnostic potential of ultrasensitive FCS for the life sciences has been discussed and demonstrated (Eigen and Rigler, 1994; Schwille et al., 1997a,b; Maiti et al., 1997). The simplicity of the measurement process, allowing data recording times down to seconds, has recently even encouraged biotechnological applications leading to fast enzyme screening (Kettling et al., 1998; Koltermann et al., 1998) in combination with the dual-color cross-correlation variant (Schwille et al., 1997b). By temporal analysis of small spontaneous deviations from the average fluorescence emanating from small illuminated ensembles, the parameters determinable by FCS include particle concentration, diffusion coefficients (Magde et al., 1972; Aragón and Pecora, 1976), flow rates (Magde et al., 1974), aggregate formation (Palmer and Thompson, 1987), kinetic rate constants of fast reversible (Magde et al., 1972; Bonnet et al., 1998; Haupts et al., 1998) and slow irreversible reactions (Kinjo and Rigler, 1995; Schwille et al., 1997a), and triplet lifetimes and populations (Widengren et al., 1995). Thus the kinetics and thermodynamics of a wide spectrum of processes accompanied by reversible fluorescence changes are accessible by FCS.

Nevertheless, few intracellular applications of FCS have been reported to date (Berland et al., 1995; Politz et al., 1998; Brock et al., 1998). The majority of correlation spectroscopy measurements in cellular systems have been performed on cell surfaces by conceptually different strategies such as scanning or imaging FCS (Petersen, 1986; Petersen et al., 1993; Koppel et al., 1994; Huang and Thompson, 1996) or correlations of the trajectories of individual molecules (Ghosh and Webb, 1994; Feder et al., 1996). These methods utilize spatial number fluctuations without a fixed measurement volume for the analysis of molecular mobility, particle binding and aggregation, but yield dynamic information with a resolution of milliseconds at best.

Anticipated problems of utilizing FCS for intracellular measurements were degraded signal-to-noise ratios due to scattering, autofluorescence, photobleaching of the dyes in restricted compartments, and cell damage resulting from the required high local doses of laser illumination. Similar problems in imaging techniques such as laser scanning microscopy have been efficiently solved by employment of

*Received for publication 24 February 1999 and in final form 25 June 1999.*

Address reprint requests to Prof. Watt W. Webb, School of Applied and Engineering Physics, Cornell University, 212 Clark Hall, Ithaca, NY 14853. Tel.: +1-607-255-3331; Fax: +1-607-255-7658; E-mail: www2@cornell.edu; or Dr. Petra Schwille, Experimental Biophysics Group, Max Planck Institute for Biophysical Chemistry, Am Fassberg, D-37077 Göttingen, Germany. E-mail: pschwil@gwdg.de.

Dr. Haupts' present address is SmithKline Beecham, Harlow, England.

Dr. Maiti's present address is Tata Institute of Fundamental Research, Colaba, Mumbai 400 005, India.



0006-3495/99/10/2251/15 $2.00

nonlinear excitation (Denk et al., 1990; Xu and Webb, 1997). It has been demonstrated that in optically thick specimens, two-photon excitation (2PE) and three-photon excitation (3PE) of dyes considerably reduce cell damage and image degradation due to scattering (Williams et al., 1994). So far, only a few attempts have been made to combine 2PE or multiphoton excitation (MPE) with FCS (Berland et al., 1995; Brand et al., 1997), presumably due to the requirement for more sophisticated pulsed laser systems, while conventional FCS can be performed with rather inexpensive continuous-wave HeNe, argon ion, or diode lasers. Nevertheless, new developments in user-friendly laser technology and the growing interest in time-resolved methods for biological specimens are likely to encourage a more widespread use of pulsed excitation and MPE.

The present study discusses the special requirements of intracellular FCS applications and presents results in several cell types to demonstrate the power of the method. Comparison of the features of confocal 1PE and 2PE is carried out using two representative dyes commonly selected as in vivo probes for their achievable signal-to-noise ratios in FCS: tetramethylrhodamine (TMR) and the photochemically enhanced red-shifted mutant of green fluorescent protein (EGFP). The dye characteristics are first determined in solution measurements before intracellular environments of several types of mammalian cells and plant cells are accessed.

## THEORY

### Two-photon excitation

With 2PE we describe the simultaneous absorption of two photons of approximately twice the wavelength or half the energy required for a transition to the excited state. Simultaneous ($\sim 10^{-15}$ s) absorption within the cross section of the dye molecule ($\sim 10^{-16}$ cm$^2$) requires high instantaneous photon flux densities on the order of $10^{31}$ photons/cm$^2$s, usually obtained from mode locked lasers providing short pulses ($\sim 10^{-13}$ s) with a high repetition rate ($\sim 10^8$ Hz). The excitation probability is proportional to the mean square of the intensity, which results in inherent depth discrimination. Because the intensity squared declines with the distance $z$ from the focal plane as $z^{-4}$, only the focal plane receives sufficient intensity for significant absorption. This allows specific illumination of interesting sites in the living cell and eliminates photodamage effects in off-focus areas. In conventional 1PE confocal microscopy, where spatial resolution is obtained by inserting a small aperture (pinhole) in the image plane, out-of-focus fluorescence is rejected but excitation still occurs all along the double cone-like profile of a focused laser beam.

Although the emission spectra of dyes remain basically the same for 1PE and 2PE, the absorption spectra can differ considerably (Xu et al., 1996). It is hardly possible to predict the 2PE wavelength maxima. The spectra are often blue-shifted with respect to twice the 1PE wavelength and broader than their one-photon counterparts, which allows simultaneous excitation of several spectral emission separable dyes, but also might be expected to enhance the danger of nonspecific excitation of the autofluorescent background, especially in the cellular environment.

### Fluorescence correlation spectroscopy

Temporal autocorrelation analysis provides a measure of the self-similarity of a time series signal and thereby describes the persistence of information carried by it. Thus any process that generates a measurable change in fluorescence can be analyzed. When performed in the illuminated focal point of a microscope objective, the time window for the investigation of particle dynamics is limited by the residence time of fluorescent particles in this open measurement volume, as determined by molecular motion. Although FCS was originally derived for the analysis of minute spontaneous fluctuations (Magde et al., 1972) and so far has been applied mostly at millisecond time scales and below, the residence time and thereby the overall correlation decay time can be considerably longer if cellular and membrane systems with slow particle diffusion are investigated.

The normalized fluorescence fluctuation correlation function is defined as

$$G(\tau) = \langle \delta F(t)\delta F(t+\tau)\rangle / \langle F(t)\rangle^2. \quad (1)$$

The raw data for FCS analysis are fluorescence fluctuations $\delta F(t) \equiv \mathrm{F}(t) - \langle F(t)\rangle$ resulting from whatever process is occurring in an open ensemble of molecules of an average concentration $\langle C\rangle$ in a detection volume $V$, illuminated by focused laser light. For 1PE, they are given by

$$\delta F_1(t) = \kappa \langle I_0\rangle \int_{\mathrm{V}} S_1(\underline{r})\Omega_1(\underline{r})\delta(q\sigma_1 C(\underline{r}, t)) \cdot \mathrm{d}V. \quad (2)$$

and for 2PE by

$$\delta F_2(t) = \frac{1}{2}\kappa g_2 \langle I_0(t)\rangle^2 \int_{\mathrm{V}} S_2{}^2(\underline{r})\Omega_2(\underline{r})\delta(q\sigma_2 C(\underline{r}, t)) \cdot \mathrm{d}V. \quad (3)$$

In these equations, $\kappa$ denotes the overall detection efficiency of the optical system (collection optics, filters, and detector), and $q$ is the fluorescence quantum yield of the dye that is considered to be equal for both excitation alternatives by including the factor ½ in Eq. 3 for the two-photon process. The excitation cross sections for 1PE and 2PE are $\sigma_{1,2}$, respectively. $\langle I_0(t)\rangle$ is the average intensity at the geometrical focal point, and $S_{1,2}(r)$ is the dimensionless spatial distribution functions of the focussed light in the sample space for either excitation wavelength. 2PE depends on $\langle I_0{}^2(t)\rangle$, so the second-order temporal coherence $g_2 = \langle I_0^2(t)\rangle / \langle I_0(t)\rangle^2$ proportional to $(\tau_\mathrm{p} f)^{-1}$ with pulse duration $\tau_\mathrm{p}$ and repetition rate $f$ is introduced to measure the 2PE efficiency by pulsed excitation. $\Omega(\underline{r})$ (often referred to as $CEF(\underline{r})$) is the collection efficiency function, another dimensionless

weighting factor for confocal optics (as first reported by Koppel et al., 1976) determined by objective and pinhole transfer properties (Qian and Elson, 1991; Rigler et al., 1993). Because $\Omega(\underline{r})$ is defined for the emission light, it does not depend directly on the excitation mode (1PE versus 2PE). With its inherent depth discrimination property, 2PE in principle requires no pinhole at all, in which case $\Omega(\underline{r}) = 1$. However, the avalanche photodetector used in this study has an active surface diameter of less than 200 $\mu$m that restricts wide-field collection and acts as a relatively large noncritical pinhole.

Temporal variations of the excitation light can be neglected in the fluorescence correlation spectra for both cases, because the 100-fs pulses at a 80-MHz repetition rate are too fast to be temporally resolved in our system. The most prominent contributions to $\delta F(t)$ are just number fluctuations due to the motion of particles through the spatially inhomogeneous illumination without a change in their fluorescence characteristics: $\delta(q_i\sigma_i C(\underline{r}, t)) = q_i\sigma_i\delta C(\underline{r}, t)$.

## Analysis of molecular dynamics

If no intramolecular dynamics affect the fluorescence of observed molecules, the autocorrelation functions just describe the motion of particles in different environments. In cellular applications, we expect at least three types of molecular motion: free three-dimensional (3D) diffusion, two-dimensional (2D) diffusion on membranes, and active, flow-like transport. In addition, the formalism of anomalous (restricted) subdiffusion with nonlinear time dependence of the mean square displacement $\langle \Delta r^2 \rangle \propto t^\alpha$, $\alpha < 1$, may be necessary to fully describe situations in and on real cells (Schwille et al., 1999). With Gaussian approximations for the convolution factors $S(\underline{r})*\Omega(\underline{r})$ (respectively $S^2(\underline{r})*\Omega(\underline{r})$) in Eqs. 1 and 2 (see the Appendix for the correct expressions), the general correlation curves for $n$ noninteracting species of concentrations $C_n$ with the same fluorescence but different diffusion or transport properties are given by

$$G(\tau) = V_{\text{eff}}^{-1}\sum_n \langle C_n\rangle M_n(\tau) \Big/ \left(\sum_n \langle C_n\rangle\right)^2 \tag{4}$$

with

$$M_n(\tau) = (1 + \tau/\tau_{d,n})^{-1}(1 + r_0^2\tau/z_0^2\tau_{d,n})^{-1/2}$$

for free 3D diffusion (4.1)

$$M_n(\tau) = (1 + \tau/\tau_{d,n})^{-1} \quad \text{for free 2D membrane diffusion} \tag{4.2}$$

$$M_n(\tau) = \exp(-(\tau \cdot v/r_0)^2)$$

for active lateral transport with velocity $v$. (4.3)

$r_0$ and $z_0$ are the characteristic lateral and axial volume dimensions, $\tau_{d,n} = r_0^2/8D$ are defined as the average lateral diffusion times for a molecule of species $n$ with diffusion coefficient $D_n$ through the effective measurement volume element $V_{\text{eff}}$. (The difference in the conventional 1PE value of $\tau_d = r_0^2/4D$ results from the introduction of the convolution factor as a squared instead of a simple Gaussian. This is a necessary requirement for an analogous treatment of 1PE and 2PE FCS, as explained in the Appendix.) For anomalous subdiffusion with $\alpha < 1$, the expression $\tau/\tau_{d,n}$ is replaced by $(\tau/\tau_{an,n})^\alpha$ (Feder et al., 1996). No conventional diffusion constant can be defined in this case, and $\tau_{an,n}^\alpha = r_0^2/2\Gamma_n$, where $\Gamma_n$ is a transport coefficient of fractional time dimension. The total number of molecules $\langle N\rangle$ contributing to the signal at any time is just the inverse amplitude of the correlation curve $\langle N\rangle = V_{\text{eff}}\Sigma_n\langle C_n\rangle = G(0)^{-1}$. With known $\langle C\rangle$ and $D$, $V_{\text{eff}}$, $r_0$, and $z_0$ can thus be determined experimentally from the correlation curves. The definition used for $V_{\text{eff}}$ is given in the Appendix.

A variety of faster processes that may occur during the molecular residence time and reversibly change the fluorescence introduce additional multiplicative exponential decay terms to the correlation function. One common example is the intersystem crossing from the first singlet to the first triplet excited state. This effect can be observed for many fluorophores at high illumination intensities as an additional shoulder on the correlation curve in the microsecond range (Widengren et al., 1995). Another interesting process that we have been studying in detail is the pH-dependent reversible protonation of the EGFP chromophore in buffer solution leading to short dark states with relaxation times in the 100-$\mu$s regime (Haupts et al., 1998). This process has the capability to provide internally calibrated pH measurements in the intracellular environment (Schwille and Pyenta, unpublished observations).

## Signal-to-noise and background considerations

The appropriate criteria for comparing various excitation schemes and fluorescence markers are signal-to-noise (S/N) ratios and background phenomena. As an extremely sensitive fluorescence technique, FCS is susceptible to known noise sources such as intrinsic photon shot noise dependent on the average count rate, excitation power instabilities, laser light that is not fully suppressed, Raman scattering, and background fluorescence. Steady background arising from solvent or fixed fluorescent particles introduces a constant error factor at all time scales in the correlation curve $G(\tau)$ that leads to wrongly decreased apparent amplitude values $G(0)$, which then overestimates $\langle C\rangle$ but does not affect the temporal information derived from it. The same error can be observed for inefficient fluorophore excitation that contributes only single photons during molecular residence times in the measurement volume. In the case of mobile, strongly fluorescent contaminants or bright native fluorophores in cells, additional background correlation spectra arise that also modify $G(\tau)$. Although most aspects of S/N ratios and background in FCS applications have been discussed previously (Koppel, 1974; Qian, 1990; Thompson, 1991; Kask et al., 1997), a short summary is required

for proper characterisation of two-photon systems and to meet the specific requirements for intracellular applications with a dynamic range from several microseconds to several seconds. While shot noise predominantly affects data quality in short time ranges in the correlation curves, background scattering and fluorescence may alter the measured curve as a whole as mentioned above and therefore have to be carefully considered.

With respect to systematic or photon shot noise, the S/N ratio for any delay time $\tau$ in FCS measurements is originally defined as the ratio of the ideal value and the standard deviation of the measured value of $G(\tau)$ (Koppel, 1974). This S/N value is dependent on the total averaging time (i.e., measurement time $T_m \gg \tau$), so that noisy data can be enhanced by longer recording. However, as shown by Koppel (1974), the crucial parameter for the control of systematic noise is the number of photons per sampling period that can be collected per single observed molecule $\eta$ rather than the total amount of measured fluorescence. With $\eta$ being the count rate per molecule, the strategy for obtaining good data quality is therefore to maximize $(\eta \cdot \tau)$. The part of the correlation curve primarily affected by photon shot noise is the region of small $\tau \rightarrow 0$ due to the required short sampling intervals, as can easily be seen in the measurement curves in Figs. 4–8. In this regime, where $(\eta \cdot \tau) \ll 1$, the S/N ratio is directly proportional to $\eta$ (Koppel, 1974; Qian, 1990; Kask et al., 1997) and should thus be enhanced by high excitation rates. For greater times $\tau$ and longer sampling, the S/N dependence on $\eta$ becomes less critical, and lower excitation intensities are required to obtain $(\eta \cdot \tau) \approx 1$. This property is important for the study of slow intracellular or membrane dynamics. For all $\tau$, there exists a square root dependence of S/N on the total averaging time: S/N $\approx T_m^{1/2}$ (Kask et al., 1997).

The amplitude of the corrected correlation curve $G(0)$ is the inverse of the average number of molecules $\langle N \rangle$ simultaneously present in the effective volume element. Thus the number of photons per molecule per second $\eta$ is just the product of $G(0)$ with $\langle F \rangle$ the average count rate in $10^3$ counts per second (kcps) reported from the detector. The determination of $\eta = G(0)\langle F \rangle$ is important in two respects: 1) it yields absolute values of the detected fluorescence per molecule that are not affected by local changes in the fluorophore concentration, and 2) it defines a relative S/N ratio for the crucial fast time scale of the correlation curve and thereby a criterion for signal quality. The value of $\eta$ depends directly on excitation rates and thus is also limited by the maximum allowable intensity values.

The effect of a steady background signal $F_B$ from unwanted quasistationary light sources on the correlation curve that is equally present at all times is not being resolved in temporal analysis because $F_B$ only contributes to the denominator in Eq. 1. With measured fluorescence $\langle F_{meas} \rangle = \langle F \rangle + \langle F_n \rangle$, the apparent number of molecules $\langle N_{meas} \rangle$ is higher than the actual value $\langle N \rangle$, which leads to an underestimation $\eta_{meas}$ for the actual $\eta$ that is given by (Koppel, 1974; Thompson, 1991)

$$\eta = \eta_{meas}\langle F_{meas} \rangle^2 / (\langle F_{meas} \rangle - \langle F_B \rangle)^2. \quad (5)$$

In almost all live cell systems, the situation can be slightly more complicated because, in addition to constant background, autofluorescence contributions to $F_B(t)$ may arise from mobile native fluorophores stable enough to be correlated themselves. The correlation of background dynamics is in this case just additive to the signal correlation:

$$G_{tot}(\tau) = \frac{C_S M_S(\tau) + C_B M_B(\tau)(\eta_B/\eta)^2}{V_{eff}(C_S + C_B\ \eta_B/\eta)^2} \quad (6)$$

(for simplicity here for a single observed dye species), where $C_{S,n}$ and $C_B$ are the concentrations of dye (S) and autofluorescent molecules (B), and $M(\tau)$ describes the dimensionless correlation function of their molecular dynamics, in the easiest case of simple diffusion (Eq. 4.1). The crucial parameter $\eta_B/\eta$ represents the weighting of background contribution, comparing the count rates per molecule of the autofluorescence sources with that of the investigated labels.

In this study, first the dependence of $\eta$ on the excitation intensity is tested for prominent cell markers like rhodamine and green fluorescent protein, with both 1PE and 2PE. A comparison of absolute measured values in the same optical setup allows a discussion of the advantages of either excitation alternative. Ideally, one might predict that with appropriate intensity levels, the same $\eta$ could be achieved with both alternatives if the efficiency of detection optics is the same, which is assumed here. However, earlier studies on two-photon FCS (Brand et al., 1997) as well as single-molecule fluorescence applications (Sanchez et al., 1997) report an unexpected limitation on fluorescence emission for 2PE of selected labeling dyes that could be due to different photophysical behavior. Because no systematic data on this topic can be found in the FCS literature, careful studies of the selected dyes were carried out in solution before accessing intracellular systems.

In cellular applications, the excitation powers have to be kept low enough not to endanger the cell or interfere with its functions and to prevent the dyes from photobleaching. In the intracellular environment, diffusion may be slowed down by high viscosities or local confinement of the labels. As a consequence, the risk of bleaching the molecules during their dwell time in the illuminated area increases, which can result in considerable errors determining the diffusion properties (Widengren and Rigler, 1996). As discussed above, the S/N ratios for very short correlation times (microsecond range) can be rather poor under low-intensity conditions. This complicates the analysis of extremely fast processes in cellular environments but does not affect the analysis of slow dynamics such as diffusion. Due to the square root dependence of S/N on $T_m$, intracellular applications may thus require data collection times $T_m$ of several minutes per correlation curve, compared to several seconds in conventional (solution) FCS measurements. However,

the limited dye resources confined in cells may be depleted by bleaching during long $T_m$ and long-term signal loss may occur, resulting in increasing amplitudes of the correlation curves and a possible drift of the measured fluorescence signal. A consideration of tolerable power level $P$ as well as total doses ($P \times T_m$) is therefore essential.

## MATERIALS AND METHODS

### Setup

The experimental apparatus is realized in a modified Zeiss IM-35 inverted microscope, using the camera port for FCS detection (Fig. 1). Parallel laser light illuminates a Nikon 63 × 1.2 NA water immersion objective. The back aperture is slightly overfilled, creating a diffraction-limited focal spot ~0.5–1 μm in diameter (depending on wavelength). For 1PE, the axial resolution has to be obtained by setting a confocal pinhole of variable diameter in the image plane. A convenient way to do this is to couple the avalanche photodiode for detection (EG&G SPCM-200 FC) to a multimode optical fiber (OZ Optics, Carp, Canada; fiber entrance in image plane), with the possibility of selecting and exchanging the core diameter. In the 2PE measurements, a fiber diameter of 100 μm (10 optical units (ou) at 580-nm emission as defined by Sheppard and Matthews (1987)) was chosen, which is large enough not to restrict the detection in the absence of light scattering. For 1PE on EGFP (Clonetech, Palo Alto, CA) we excite at 488 nm with an argon ion laser (model 5425; Ion Laser Technology, Salt Lake City, UT), using a Chroma Technology (Brattleboro, VT) dichroic beamsplitter 498/DRLP and a bandpass filter HQ530/50. 1PE measurements on cell staining probes ODR, CMTMR (Molecular Probes), and Cy-3 (Amersham, Piscataway, NJ) labeled IgE antibody (a gift of D. Holowka and B. Baird, Department of Chemistry) are performed with excitation at 543 nm with HeNe model 1052 (Uniphase, San Jose, CA), using a Chroma dichroic 530/DRLP and a D580/50 filter. The two-photon experiments are carried out with 80-MHz, 100-fs pulsed excitation of a mode-locked tunable Spectra Physics (Mountain View, CA) Tsunami titanium-sapphire laser, using a Chroma short-pass dichroic 750/DCSP and two Chroma D575/150 filters for efficient suppression of IR excitation light. The dyes are excited at their two-photon absorption maxima: TMR at 850 nm, EGFP at 920 nm. The detector signal is correlated online by the ALV-5000E correlator board (ALV, Langen, Germany). Autofluorescence spectra were taken with a Spex (Edison, NJ) 270-M fiber-coupled spectrometer in confocal detection mode. The filters used here were a 510-nm glass filter (Schott) and an additional HQ680SP short-pass filter for 2PE (Chroma). The excitation power dependence of $\eta$ for EGFP and TMR was measured in aqueous solutions of both dyes (EGFP at pH 8) by first exciting with one photon and using the 25-μm pinhole for detection, then changing the illumination source, dichroic mirror, and fiber diameter for two-photon measurements. The specimens were 2 ml of 50 nM solutions in sealable plastic chambers with a coverslip bottom to guarantee concentration stability.

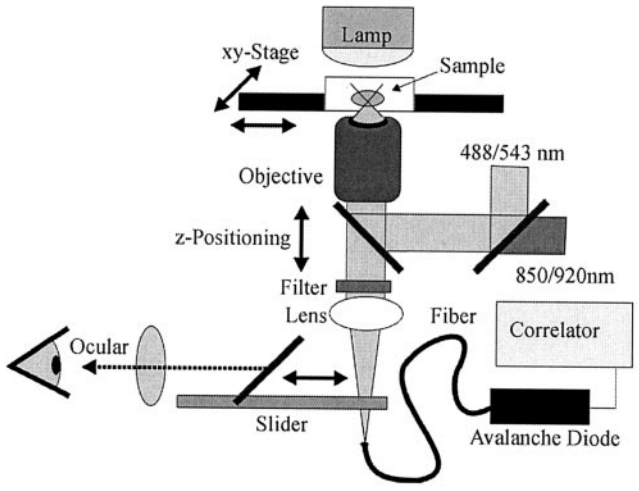


FIGURE 1 Optical setup of FCS experiments as realized in an inverted Zeiss IM35 microscope. The measurement volume is defined by illuminating the back aperture of a microscope objective with a parallel laser beam of chosen wavelength, and for 1PE by the diameter of the multimode fiber in the image plane. The positioning of the volume in the cell is done by moving the sample stage. A slider allows either observation of the cells by regular wide-field microscopy or detection of fluorescence with an avalanche photodiode for FCS measurements.

### Cell preparation

RBL-2H3, HeLa, and EMT6 cells are seeded into 35-mm coverslip-bottom microwells (MatTek Corp., Ashwell, MA) at 2 × $10^5$ cells per well in Phenol-Red-free culture medium. The cells are allowed to adhere overnight at 37°C in a 5% $CO_2$ incubator. For the FCS experiments with rhodamine/Cy-3 antibody probes, 1–5 μl of 1 μg/ml dye equivalent was added to the ~3 ml media in the dish and incubated for 5 min. Immediately before the experiment, cells are rinsed several times with phosphate-buffered saline. In the FCS measurements we determine the achieved dye concentration in the cells, mostly between 20 and 100 nM in RBL and HeLa. EMT6 exhibits a significantly reduced dye uptake of concentrations almost an order of magnitude smaller under the same labeling conditions. Cellular EGFP measurements are performed on genetically transformed RBL and tobacco cells. Plant cell preparations were made from freshly cut leaves immersed in water and measured on a conventional microscope slide covered with a coverslip. The EGFP concentration varied considerably from sample to sample between 50 and 700 nM due to expression level differences.

## RESULTS AND DISCUSSION

The objective of this study is to demonstrate the application of FCS to quantitative measurements of dynamics of molecular processes in living tissues. First, a general comparison of 1PE and 2PE in terms of signal quality is important because this choice governs instrumentation. The achievable values of photon count rates per molecule $\eta$ and their dependence on excitation power are explored for the selected dyes in solution measurements before the more complex situations in live cell systems are dealt with. After that, dye diffusion in cells and on cell membranes is investigated with both excitation alternatives. Finally, experimental considerations, including signal loss effects, background, and autofluorescence of unlabeled cells are determined for appropriate optical conditions and power levels.

### Calibraton of measurement elements and choosing comparable conditions

Because the representation of a fluorescent species in the correlation curve is determined by the probability that a molecule contributes more than one photon to the signal during its observation time, another crucial parameter in FCS measurements, besides $\eta$, appears to be the size of the measurement volume, which determine mean dwell times. In 1PE, $\eta$ diminishes when small pinholes are chosen, i.e., when $V_{eff}$ and, particularly, $z_0$ are decreased. On the other

hand, the influence of scattering background increases with bigger volumes (Mets and Rigler, 1994). In addition, a Gaussian approximation for the intensity distribution is sufficiently accurate only for a limited range of pinhole diameters (Rigler et al., 1993). For every optical setup and excitation intensity, a pinhole size can be determined that maximizes $\eta$ and still obeys the conditions of proper curve fitting following Eq. 4. With the objective used and power levels below 0.5 mW (intensity of $\sim$250 kW/cm$^2$ for overfilled objective back apertures), a pinhole size of 100 $\mu$m corresponding to $\sim$10–12 optical units (ou), depending on emission wavelength, has in previous measurements appeared to be favorable for the optimization of $\eta$ in standard 1PE applications.

However, an appropriate comparison of 1PE and 2PE in terms of measured $\eta$ requires that the effective volume elements be of comparable size, i.e., that $\langle N\rangle$ ($G(0)$) and $\tau_d$ are similar when the same sample is observed. For the diffraction-limited case, theoretical calculations of the expected intensity distributions as well as experimental evidence suggest that the required pinhole size for the one-photon setup has to be considerably smaller than 50 $\mu$m/$\sim$6 ou (580 nm) for the volume to correspond to the two-photon conditions. Fig. 2 demonstrates the pinhole size dependence by showing correlation curves of a solution of EGFP, excited by 2PE at 920 nm, and excited by 1PE at 488 nm with three different detection pinhole sizes. It can easily be verified that although the curves differ slightly in shape, the one-photon correlation curve with the smallest (25 $\mu$m/$\sim$3 ou) pinhole best duplicates the two-photon conditions. Correlation amplitudes as well as decay times are similar, indicating that the two volumes contain the same number of molecules $\langle N\rangle$ with almost identical residence times $\tau_d$. For the larger pinholes, $\langle N\rangle$ and $\tau_d$ increase. A pinhole size of 25 $\mu$m is therefore chosen in one-photon measurements to compare 1PE and 2PE in FCS solution measurements and to achieve the same resolution for cellular applications. This value of confocal aperture cancels out the effects of wavelength difference to generate the closest equivalent point spread functions for the two methods. Under these conditions, we have an effective ellipsoidal volume element of $V_{eff} \approx 0.3 \times 10^{-15}$ liters in both cases with radial half-axes $r_0 = (8D\tau_d)^{1/2} \approx 0.4$ $\mu$m. The pinhole size of 25 $\mu$m corresponds to 3 ou (510 nm) for EGFP and 2.7 ou (575 nm) for TMR emission. Values between 2.8 and 3.3 ou have previously been determined to give ideal S/N conditions in confocal scanning applications (Sandison and Webb, 1994; Sandison et al., 1995).

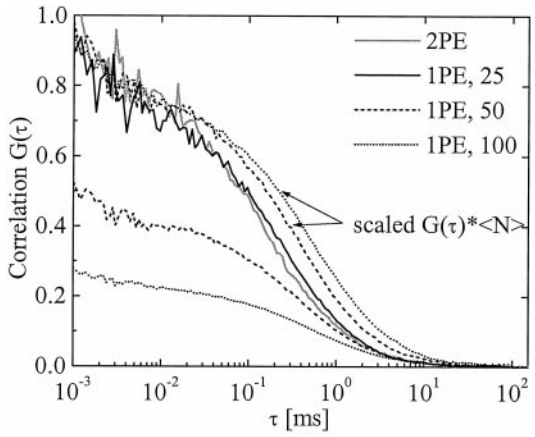


FIGURE 2 FCS curves of EGFP in pH 8 buffer measured by 2PE (*gray*) and by 1PE (*black*) with different pinhole sizes (*solid curve*, 25 $\mu$m; *dashed curve*, 50 $\mu$m; *dotted curve*, 100 $\mu$m). The initial amplitude of the solid curves $G(0)$ corresponds to the inverse mean number of molecules $\langle N\rangle$ contained in the so defined volume element $V_{eff}$. The times $\tau$ corresponding to half-maximum values of $G(0)$ indicate the average molecular residence, here diffusion times $\tau_d$. The big pinhole curves are scaled to the same $G(0)$ to better compare $\tau_d$. It can easily be verified that the 25-$\mu$m size best duplicates the focal volume geometry of the two-photon case, because both amplitudes $G(0)$ and the residence times $\tau_d$ are similar.

## In-solution measurements

### *Comparison of 1PE and 2PE in terms of $\eta$*

Two dyes of particular interest for intracellular applications of FCS are tetramethylrhodamine (TMR) and EGFP, the enhanced red-shifted mutant of the green fluorescent protein. The first is probably the best studied and most applied dye in FCS measurements to date, with known counting rates per molecule $\eta$ up to 200 kcps/molecule in a well-designed apparatus with high detection efficiency, and with a large variety of labeling possibilities for many kinds of biologically active molecules (Haugland, 1996). GFP mutants, on the other hand, have become the most powerful labeling tools in molecular biology at present, because of the ability to introduce them into the genome and specifically target them to interesting proteins in a variety of cell lines (Tsien, 1998).

Fig. 3 *a* shows the excitation power dependence of $\eta$ for EGFP, and Fig. 3 *b* shows it for TMR. The *y* axis parameter $\eta$ in $10^3$ photons/s (kcps) is held the same for both excitation alternatives, while the excitation power axes are scaled for best overlap at low power. The two-photon power is squared to represent the underlying process. In the case of EGFP in Fig. 3 *a*, the power dependencies of $\eta$ for both excitation methods can be brought to an almost perfect overlap, suggesting that at proper power levels 2PE allows an equivalent S/N quality of FCS measurements over almost the whole range. For 1PE, a correction for solvent Raman scattering background had to be included following Eq. 5. In the two-photon measurements, however, the IR Raman background can easily be discriminated experimentally. The linear (or quadratic, respectively) power dependence is observed up to values of $\eta \approx 5$ kcps/molecule, then a deviation due to excited state saturation and/or photobleaching sets in. The maximum $\eta$ that could be reached for EGFP is $\sim$15 kcps/molecule, far below the saturation expected for singlet-state excitation. Because the limit is the same for continuous 1PE and pulsed 2PE, slow processes such as

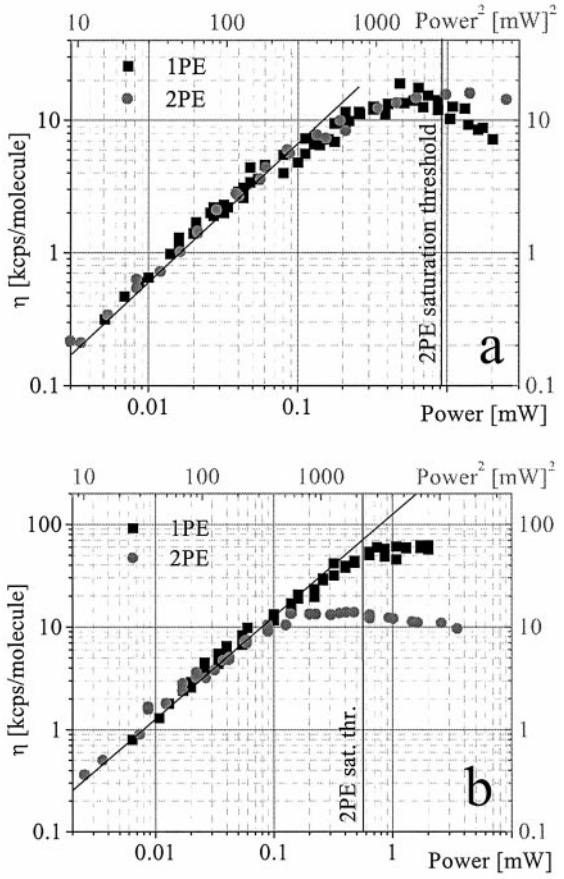


FIGURE 3 Power dependencies of single molecule emission rates $\eta$ for EGFP (*a*) and TMR (*b*), as measured in aqueous solution with a 60 × 1.2 objective and the 25-$\mu$m pinhole in the 1PE case. Linear (quadratic) slope is plotted for comparison. *Black squares*, 1PE; *gray circles*, 2PE. Estimated saturation limits for 2PE due to pulsed excitation assuming the relationship $g\sigma_2 I^2/2 = f$ are indicated by vertical lines. For TMR, a significant difference between 1PE and 2PE for the onset of deviations from the linear dependency indicates a population of long-living (>12 ns) states by 2PE.

intersystem crossing to the triplet state are assumed to limit the fluorescence output.

For TMR as plotted in Fig. 3 *b*, however, the 2PE curve deviates from the linear regime at much lower levels of $\eta$ than the 1PE curve. While the 1PE curve stays linear up to 20 kcps/molecule and reaches maximum values of 70 kcps/molecule, the two-photon curve shows a sudden plateau just above 13–15 kcps/molecule. To test whether saturation effects due to the pulsed excitation with comparably long "silent" periods of 12 ns between pulses could be responsible for the limitation, a pulse repetition rate doubler was built and applied. No significant change could be observed (Schwille et al., unpublished observations), suggesting that excited states with lifetimes longer than 12 ns are populated by 2PE. Anomalous photophysical behavior of this dye with 2PE at high power has previously been suggested by other groups (Sanchez et al., 1997; C. Seidel, personal communication). The origin of this effect will be a topic of future investigations. It is worth noticing that TMR in contrast to EGFP is excited at a rather blue-shifted two-photon absorption maximum of 850 nm (corresponding to 425 nm by 1PE) relative to the one-photon maximum at 543 nm.

The special kind of *a posteriori* representation in Fig. 3 with the criteria $\eta_1 = \eta_2$ ($F_1 = F_2$) at low power allows an independent estimation on a single-molecule scale of the two-photon cross section $\sigma_2$, relative to the one-photon cross section $\sigma_1$, provided that all other parameters in Eqs. 2 and 3 are known and the measurement volumes are of a comparable size, which has been demonstrated above. Although $\sigma_2$ for related dyes like rhodamine B, wild-type GFP, and the mutant S65T have been reported (Xu and Webb, 1997), FCS offers an interesting measurement alternative based on fluorescence per single molecule. Under the assumption of equal $V_{\text{eff}}$, $\langle N\rangle$, $q_1 = q_2$, the illumination intensities necessary to fulfill $F_1 = F_2$ yield

$$\sigma_2 \approx 2\sigma_1\langle I_{0,1}\rangle/g_2\langle I_{0,2}(t)\rangle^2. \quad (7)$$

With measured values $\sigma_1(\text{EGFP}) = 2 \times 10^{-16}$ cm$^{-2}$ and $\sigma_1(\text{TMR}) = 3 \times 10^{-16}$ cm$^{-2}$, as well as $g_2 \approx 7.5 \times 10^4$, we determine $\sigma_2(\text{EGFP}) \approx 180$ GM and $\sigma_2(\text{TMR}) \approx 200$ GM, corresponding sufficiently well with cross sections determined in our group by conventional methods (Xu and Webb, 1997; Heikal et al., unpublished observations).

At power levels well below the saturation or photobleaching limits that are used for all following intracellular applications, below 0.1 mW (one-photon) and 15 mW (two-photon), we conclude that neither of the selected dyes shows a significant difference in the values of $\eta$ that can be achieved by 1PE or 2PE. The power dependence is linear or quadratic, as expected. This suggests that 2PE under comparable measurement conditions, i.e., same volume element size and spatial resolution, does not show any drawbacks in terms of FCS signal quality at appropriate excitation intensities. However, one must keep in mind that for 1PE higher $\eta$ can be achieved in solution close to saturation by using bigger measurement volumes $V_{\text{eff}}$ as achieved with larger pinholes and reduced spatial resolution ($\eta$ = 150 kcps/molecule for TMR, 60 kcps/molecule for EGFP in our setup with 100-$\mu$m pinholes). In all FCS applications, there is a temptation to choose excitation intensities close to the excited-state saturation levels of the fluorophores (Figs. 3), because $\eta$ is thus maximized. However, the apparent nonlinearities in these regimes often introduce severe errors in quantitation of $\tau_d$ and $\langle N\rangle$ or $\langle C\rangle$.

## Cellular applications

The following intracellular applications with 1PE and 2PE are designed to determine the molecular mobility of probe molecules in cellular compartments, but also to compare $\eta$ as well as autofluorescence and background parameters $F_B$, $C_B$, $\eta_B$, and $\tau_B$ in Eqs. 7 and 8 for the range of excitation intensities that revealed equal $\eta$ in the solution studies. We attempt to determine whether it is useful to enlarge the pinhole from 25 $\mu$m to 100 $\mu$m and to decrease resolution to achieve higher $\eta$, as shown by in-solution measurements.

Finally, because it has to be guaranteed that the cell damage power threshold is not reached by either excitation alternative under favorable illumination conditions, this limit is experimentally determined.

### *Diffusion studies*

To explore the potential of FCS measurements inside living cells and tissues, test systems have to be chosen that are sufficiently well understood to allow reliable interpretation. This suggests looking at freely diffusing dye molecules in the cytoplasm and on the cell membrane. The only published work to date employing two-photon FCS in cells (Berland et al., 1995) has investigated the diffusion characteristics of fluorescently labeled latex spheres that had been inserted into fibroblast cells by electroporation. The high labeling density of these spheres provides good S/N levels; however, the investigation of biochemically relevant molecular processes in cells requires single dye molecule sensitivity. For this reason, we investigate concentrations of individual dye molecules in the 10 nM range and choose labels that can be taken up by living cells without perforating them.

For a representative study of the range of time dynamic scales that can be investigated, we applied rhodamine derivatives: cell tracker orange CMTMR (Haugland, 1996), designed to stain the cytoplasm by irreversibly permeating the cell membrane, and the lipid probe octadecyl rhodamine (ODR) (Haugland, 1996), which inserts specifically into cell membranes. Three sustained culture mammalian cell lines were investigated: rat basophilic leukemia (RBL) cells, frequently used for immunological signaling research, and HeLa and EMT6, two transformed tumor lines. For RBL cells, we also applied a multiply Cy-3-labeled IgE antibody to investigate the diffusion of IgE receptor on the cell membrane.

Fig. 4 shows the results of diffusion measurements inside and on the plasma membranes of RBL cells, performed with 1PE at 543 nm and 10–60 $\mu$W, with 100-$\mu$m and 25-$\mu$m pinholes, and equivalent measurements with 2PE at 850 nm at 6–10 mW. For comparison of the time scales and to calibrate the system, the solution measurement of TMR ($D = 2.8 \times 10^{-6}$ cm$^2$/s) is included. Power levels were chosen to maximize $\eta$ while keeping excitation in regimes where the curve shape was not power dependent, to avoid diffusion time artifacts due to photobleaching (see below). Because the decay time of the correlation curves $\tau_d$ scales inversely proportionally to $D$, it can easily be verified that the dynamic range represented in Fig. 4 is four orders of magnitude. The slowest diffusion process, IgE receptor diffusion on the membrane yielded the value $D \approx 4 \times 10^{-10}$ cm$^2$/s, which matches very well the value previously determined in FPR measurements for the same cell and receptor type (Menon et al., 1986; Feder et al., 1996). Diffusion in membranes had often been considered too slow to be conveniently measured by FCS. The 1PE (25 $\mu$m) and 2PE curves are almost identical, with decay times of a factor of 3.5 smaller than for the 1PE curves with the large 100-$\mu$m pinhole. The receptor diffusion curve for 2PE (and 1PE with a small pinhole) is missing, because Cy-3 showed a too low photophysical stability for two-photon applications in the wavelength range of 850–930 nm.

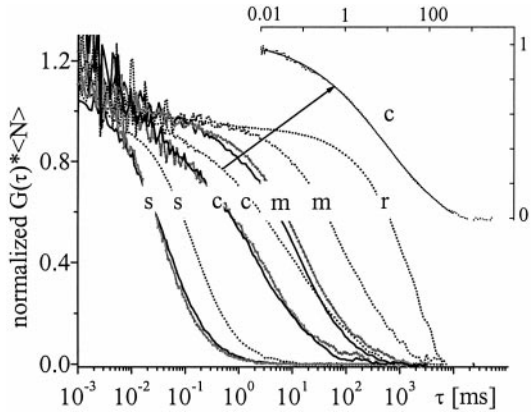


FIGURE 4 Dynamic range of FCS diffusion measurements of TMR dye in solution (s), in the cytoplasm (c), and in the cell membranes (m), and of Cy-3-labeled IgE receptors on the membrane (r), by 1PE with a 100-$\mu$m pinhole (*dotted lines*) and 2PE (*gray lines*) compared to 1PE with a 25-$\mu$m pinhole (*solid black lines*). Four orders of magnitude in residence times are easily accessible by FCS, corresponding to diffusion coefficients of $10^{-6}$ to $10^{-10}$ cm$^2$/s. The inset exemplifies the result of data fitting with the anomalous diffusion model to the intracellular curve.

By fitting the measured curves in Fig. 4 to Eq. 4 as summarized in Table 1, deviations from normal diffusion (anomalous subdiffusion) are found for all cellular environments independent of the excitation methods 1PE or 2PE, or pinhole size. On membranes, we have found reproducible values of $\alpha \approx 0.7$ for lipids (Schwille et al., 1999) and find similar values for IgE receptors. The magnitude of the 2D diffusion parameters can be approximated, however, using the values of $r_0$, $z_0$ determined by calibration with TMR in solution. An interesting observation is the unusually low slope of the CM-TMR diffusion curves in the cytoplasm that could be seen by both 1PE and 2PE in each observed cell type. These curves are highly reproducible and show only a slight dependence on the measurement position within the cell. The intracellular dynamics can no longer be reasonably approximated by free 3D diffusion with a single time constant. Instead, anomalous diffusion with values of $\alpha \approx 0.5$ or free diffusion with at least two different mobilities, $D_1$ and $D_2$, have to be assumed to fit the curves ($n = 1, 2$ in Eq. 4). In this case, $D_2$ values are found to be close to the values for membrane-bound dye. The partition coefficient between fast and slow diffusion populations varies between 30% and 50% for $D_2$, and $D_1$ is about a factor of 5 lower than for dye diffusion in buffer. Although comparable studies with cytoplasmatic EGFP in RBL cells have also shown significant differences from EGFP diffusion in buffer (a factor of 3–4 slower), they are free of contributions from a slow membrane-like diffusion and can be described by assuming a single diffusing species. This sug-

**TABLE 1 Molecular mobilities in cells and on cell membranes as illustrated in Fig. 4, assuming different fitting models, anomalous subdiffusion with $\langle \Delta r^2 \rangle = \Gamma t^{\alpha}$, and normal diffusion with two coefficients, $D_1$ and $D_2$**

| | | Cytosolic measurements with CMTMR | | | | |
|---|---|---|---|---|---|---|
| Fitting model | Fitting parameters | HeLa cytos. | EMT6 cytos. | RBL cytos. | ODR RBL membr. | Cy-3 RBL, IgE receptor |
| Anomalous diffusion [$\Gamma$] = $10^{-8}$ cm$^2$/s$^{\alpha}$ | $\Gamma$ (1PE,100) | 25 ± 7 | 40 ± 12 | 30 ± 9 | 0.8 ± 0.2 | 0.08 ± 0.05 |
| | $\alpha$ | 0.57 ± 0.12 | 0.65 ± 0.1 | 0.56 ± 0.1 | 0.75 ± 0.1 | 0.8 ± 0.1 |
| | $\Gamma$ (1PE,25) | 28 ± 12 | 42 ± 13 | 35 ± 7 | 0.9 ± 0.4 | 0.1 ± 0.05 |
| | $\alpha$ | 0.59 ± 0.15 | 0.67 ± 0.15 | 0.58 ± 0.15 | 0.78 ± 0.2 | 0.76 ± 0.2 |
| | $\Gamma$ (2PE) | 27 ± 9 | 44 ± 13 | 34 ± 12 | 0.8 ± 0.3 | n.d. |
| | $\alpha$ | 0.58 ± 0.15 | 0.67 ± 0.15 | 0.57 ± 0.15 | 0.78 ± 0.2 | n.d. |
| Normal diffusion [$D$] = $10^{-8}$ cm$^2$/s | $D_1$ (1PE,100) | 4 ± 0.7 | 20 ± 12 | 17 ± 8 | 0.5 ± 0.3 | 0.04 ± 0.03 |
| | $D_2$ | 0.1 ± 0.08 | 1 ± 0.8 | 0.8 ± 0.6 | — | — |
| | Fraction ($D_2$) | 60 ± 16% | 40 ± 10% | 40 ± 10% | — | — |
| | $D_1$ (1PE,25) | 5.6 ± 0.8 | 20 ± 14 | 18 ± 4 | 0.7 ± 0.4 | 0.05 ± 0.08 |
| | $D_2$ | 0.14 ± 0.13 | 1.3 ± 0.8 | 0.9 ± 0.5 | — | — |
| | Fraction ($D_2$) | 60 ± 17% | 33 ± 9% | 42 ± 11% | — | — |
| | $D_1$ (2PE) | 5 ± 0.5 | 20 ± 15 | 25 ± 8 | 0.9 ± 0.4 | n.d. |
| | $D_2$ | 0.15 ± 0.06 | 1.1 ± 0.8 | 1 ± 0.9 | — | n.d. |
| | Fraction ($D_2$) | 55 ± 13% | 35 ± 7% | 40 ± 12% | — | n.d. |

gests that the inhomogeneously retarded diffusion of intracellular CMTMR in cells is due to the partial interaction of this probe with intracellular structures or with much larger soluble molecules. On average, we find that the diffusion of probe molecules like EGFP and TMR is slowed down with respect to aqueous solution by a factor of 4–10 in the cytoplasm, $10^3$ on membranes, and $10^4$ when they are bound to IgE receptors, which is consistent with values reported by other investigators applying FPR (Swaminathan et al., 1997; Feder et al., 1996).

### *Spatial resolution*

The previous section has demonstrated that diffusion properties of probe molecules can be employed to study different cellular compartments including membranes and cytoplasm. The question now is, how well are these compartments spatially discriminated by our detection optics? To test the resolution properties for site-specific intracellular applications, we measured an RBL cell line that contains palmitoylated EGFP-Lyn analogs targeted to the membrane inner leaflet (P. Pyenta, D. Holowka, and B. Baird, unpublished observations), which has, as expected, a large membrane-bound fraction and smaller concentrations diffusive in the cytoplasm. In *z*-stepping into the cell as illustrated in Fig. 5, it was verified that in regions close to the cell surface, slow 2D membrane diffusion dominates the correlation curve, whereas in deeper *z* layers, the membrane diffusion could be completely suppressed, and fast 3D intracellular diffusion was observed. Because the plasma membrane is very thin (~4 nm) relative to the height of the focal volume (>1 $\mu$m), isolation of pure membrane diffusion without contributions from intracellular regions is not achievable. If diffusion time scales can be distinguished and numbers of molecules are comparable in different compartments, as is the case here, evaluation of the correlation curves, assuming Eq. 4 in the appropriate dimensionalities, reveals the characteristic parameters for both environments as well as the concentration partition.

Fig. 6 shows FCS data on diffusion curves taken at the cell surface, in the left panel with 1PE with a low-resolution 100-$\mu$m pinhole, and in the right panel with 2PE (corresponding to a 25-$\mu$m pinhole for 1PE as demonstrated). The relative contributions of intracellular dye in the case of the large pinhole are 45 ± 10% of all molecules in the volume element. With 2PE, this fraction in the same cells is reduced to 6 ± 5%. This demonstrates a remarkable axial precision obtainable without any loss in terms of $\eta$ (see Tab. 2). It is notable that by FCS evaluation of total numbers of molecules, the partition between fast and slow mobilites and

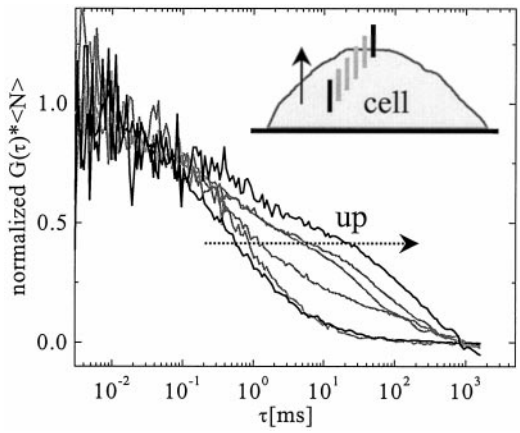


FIGURE 5 Coexisting cytoplasmatic and membrane diffusion spatially resolved: *z*-stepping with 1-$\mu$m steps (100-$\mu$m pinhole, low resolution) through a RBL cell expressing GFP-labeled palmitoylated Lyn analogs distributed in cytoplasm and on membranes. Close to the cell surface, both intracellular (fast) and membrane (slow) mobilities are represented; in deeper *z* positions, the membrane contribution can be avoided. The fast intracellular part is always present.

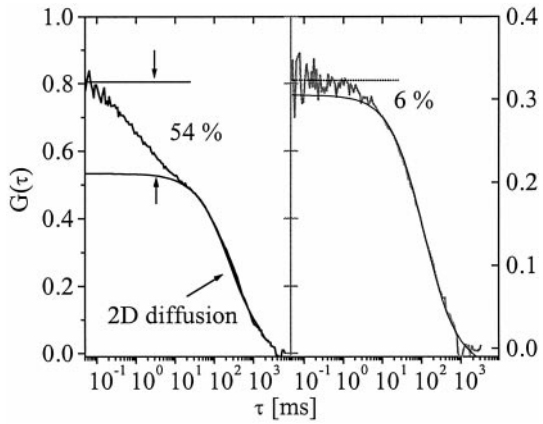


FIGURE 6 Analysis of FCS curves close to membranes, as in Fig. 5. The membrane diffusion parts of the curves are fitted by the 2D diffusion model. The suppression of intracellular diffusion is much more efficient with 2PE or a 25-$\mu$m pinhole (*right*) with only 6% fast diffusing species remaining; with a 100-$\mu$m pinhole and 1PE (*left*), 54% fast diffusing species remains.

absolute concentrations on the membrane as well as the cytoplasm can be determined contemporarily as in Eq. 4; e.g., a volume concentration of 100 nM in a femtoliter corresponds to a mole fraction of $\sim 10^{-5}$ on the membrane for comparable numbers of fluorophores in the focal volume.

### *Artifact control limits on excitation power in cellular applications of FCS*

Three unwanted effects of excessive excitation powers are to be distinguished in cellular FCS applications. These artifacts are 1) photobleaching, shrinking apparent residence times of dye molecules in the focal spot; 2) continous dye depletion in the cell interior leading to signal loss; and 3) cell damage. We define $P_{\text{diff}}$ as the power limit above which the diffusion time is underestimated, and $P_{\text{dam}}$ as the limit of cell damage visible as morphological changes. To quantify signal loss, illumination doses ($P \times T_{\text{m}}$) rather than powers have to be considered by defining a tolerable loss factor, e.g., 1/*e*, and determining the maximum measurement time $T_{\text{m}}$ to stay below this value for a given excitation power. However, to maximize signal quality, it is highly recommended to select $P$ high enough that $\eta \gg \tau_{\text{d}}^{-1}$ but necessarily below $P_{\text{diff}}$. All values, $P_{\text{diff}}$, $T_{\text{m}}$, and $P_{\text{dam}}$, are strongly dependent on the chosen dye system; the selection of dyes with high $P_{\text{diff}}$ is therefore of crucial relevance for all cellular FCS applications.

Table 2 summarizes the $P_{\text{diff}}$ and the maximum values $\eta(P_{\text{diff}})$ that could be obtained in our systems with 1PE and 2PE staying safely below $P_{\text{diff}}$ and compares them with the expected values in solution for the same power levels. Two interesting observations can be made. First, the discrepancy between in-solution and intracellular $\eta$ at the same intensities is considerably larger for 1PE, presumably due to background in cells that reduced the apparent value of $\eta$. Second, the advantage of using larger pinhole sizes for 1PE disappears for the same reason. The only case where $\eta$ and thereby the S/N could be increased detectably by reducing spatial resolution was for cytoplasmatic measurements in EMT6 cells. This result, as well as the better preservation of $\eta$ values by 2PE, suggests that the nonspecific background induced by the cells is more critical in the case of 1PE.

An even more evident advantage of using 2PE is the reduction of cumulative signal loss with irradiation doses. In one-photon applications, fluorescence is excited and photobleaching occurs all along the excitation cone. Using smaller pinholes can improve resolution properties as demonstrated, but the overall amount of excitation cannot be reduced. As a consequence, depletion due to irreversible 1PE photobleaching of dye molecules restricted to the cell interior is much more severe than for 2PE. The effects of long-term fluorescence loss are shown in Fig. 7. After an initial short illumination phase (~s) to deplete immobile background, 10 successive FCS measurements of 10 s duration are taken in individual HeLa cells loaded with CM-TMR, either by 1PE with 40 $\mu$W, or by 2PE with 9 mW. These excitation power levels are slightly below $P_{\text{diff}}$ and correspond to the same $\eta$ levels in cells (~4 kcps/molecule). In solution, we would expect 7 kcps/molecule for 1PE. While the average count rate $\langle F \rangle$ and the correlation amplitude in the two-photon case remain almost constant

**TABLE 2 Control limits for illumination power ($P_{\text{diff}}$) and data collection time $T_{\text{m}}$ in FCS measurements with rhodamine dyes, with achievable $\eta$ for these powers in cells and in solution**

| | HeLa cytosol | EMT6 cytos. | RBL cytos. | RBL membrane |
|---|---|---|---|---|
| $P_{\text{diff}}$ (1PE) | 60 $\mu$W | 60 $\mu$W | 40 $\mu$W | 10 $\mu$W |
| $P_{\text{diff}}$ (2PE) | 10 mW | 10 mW | 9 mW | 6 mW |
| $T_{\text{m}}$ ($P_{\text{diff}}$, 1/*e*) 1PE | 60 s | 30 s | 40 s | 3 min |
| $T_{\text{m}}$ ($P_{\text{diff}}$, 1/*e*) 2PE | 15 min | 5 min | 8 min | 3 min |
| | kcps/molecule | kcps/molecule | kcps/molecule | kcps/molecule |
| $\eta$ ($P_{\text{diff}}$) 1PE 100 | 4.9 ± 1.2 | 8.0 ± 2.5 | 3.9 ± 1.5 | 1.6 ± 1 |
| $\eta$ ($P_{\text{diff}}$) in solution | 18 ± 2 | 18 ± 2 | 10 ± 1.6 | 3.6 ± 0.8 |
| $\eta$ ($P_{\text{diff}}$) 1PE 25 | 3.9 ± 1.0 | 5.5 ± 1.5 | 3.9 ± 0.9 | 1.6 ± 0.8 |
| $\eta$ ($P_{\text{diff}}$) in solution | 8 ± 1.1 | 8 ± 1.1 | 6.2 ± 1.3 | 2.2 ± 1.1 |
| $\eta$ ($P_{\text{diff}}$) 2PE | 3.9 ± 1.0 | 5.6 ± 1.7 | 3.9 ± 1.0 | 1.1 ± 0.3 |
| $\eta$ ($P_{\text{diff}}$) in solution | 4 ± 1.3 | 4 ± 1.3 | 3.5 ± 1.1 | 1.5 ± 0.9 |

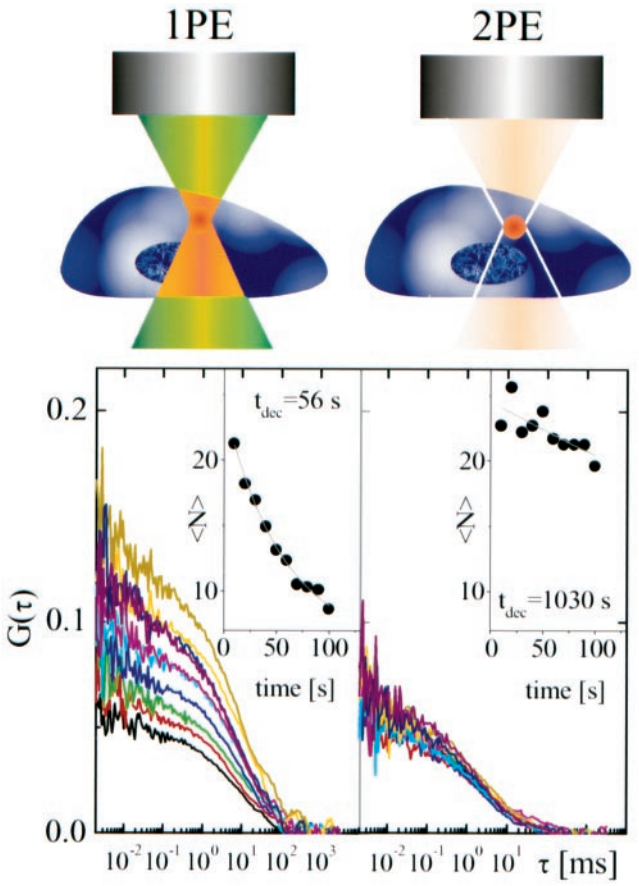


FIGURE 7 Concentration depletion of intracellular TMR due to accumulative photobleaching by the illuminating beam. Decreasing concentrations of dye can be observed as a rise in correlation amplitude with time. As a demonstration, 10 successive measurements of 10 s each are taken at the same $\eta$ levels. *Left*: 1PE with a 25-$\mu$m pinhole; the amplitude $G(0)$ increases by a factor of 2.5. *Right*: 2PE, the amplitude remains almost unchanged with a tolerance of 10%. The insets show the decay in the mean number of particles $\langle N \rangle$ with the fitted $1/e$ decay time values $t_{dec}$. *Above*: Schematic explanation of the observed effect. 1PE, on the left, excites fluorescence all along the double cone of the illumination profile within the cell, while 2PE occurs only in a small volume around the focal point.

within a tolerance of 10% (Fig. 7, *right*), the correlation amplitude increases dramatically (two- to threefold) for 1PE (Fig. 7, *left*), with a simultaneous decrease in the average count rate, indicating that the concentration of dye molecules in the cell is continuously depleted in this case. This effect in 1PE is not dependent on the detection pinhole size and clearly demonstrates that bleaching by the large illumination cone in out-of-focus regions is quite severe, even for low powers at the doses required for good S/N values. The dye depletion can be approximated by exponential decay (Fig. 7, *insets*). Table 2 compares the measurement times $T_m$ ($P_{diff}$, $1/e$) at which the signal is reduced to $1/e$ because of cumulated bleaching at $P_{diff}$. Greater loss factors might be tolerable if the absolute concentration of the dye is not a crucial parameter, escpecially at high dye load (>100 nM) and low autofluorescence levels.

### *Photodamage effects*

Long-term irreversible dye photobleaching due to limited resources occurs in every cell for all dyes to a certain extent, especially for slowly diffusing particles. Because it is usually dependent on the total illumination dose rather than on the power, there is a direct tradeoff between signal loss and the achievable S/N ratio determined by measurement duration. For this reason, 2PE applications that allow far longer averaging times $T_m$ for the same or even higher $\eta$ values are highly favorable.

Visible cell damage could not be observed at $P_{diff}$ with 1PE or for higher applied powers to ~20 times $P_{diff}$ (<2 mW) as long as the dye concentration in the cell was kept below 100 nM. For 2PE, localized morphological changes accompanied by a red-shifted bright induced autofluorescence appeared above $P_{dam}$ = 30 mW (Fig. 9 *a*), which is only three times $P_{diff}$, even without dye load.

### *Penetration of thick cell walls and whole cell layers for FCS dynamical measurements*

To test the expected advantages of 2PE regarding increased penetration depths in tissues and reduced scattering at cell surfaces, tobacco leaf epidermal tissues were chosen for an intracellular FCS study because their thick cell walls enhance scattering effects. We investigated the diffusion of a cytosolic GFP mutant S65T, with spectroscopic properties very close to that of EGFP, in tobacco plants (Köhler et al., 1997). Samples were taken from cut leaves, so that multiple cell layers, each ~10 $\mu$m thick, were accessible. Fig. 8 shows the results of intracellular GFP diffusion measurements. Scattering reduces the values of $\eta$ that could be obtained by 1PE to almost a factor of 2 lower than for 2PE,

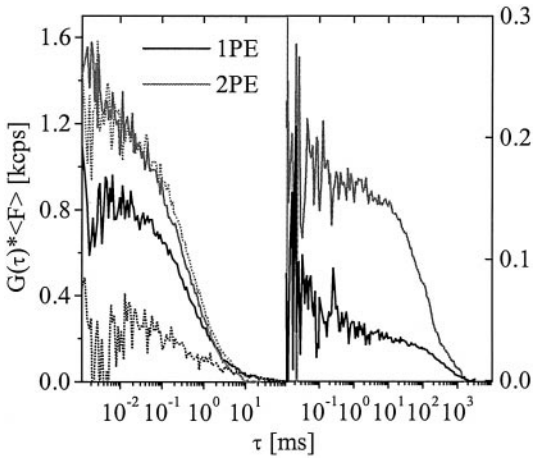


FIGURE 8 FCS in turbid tissue. *Left*: measurement of GFP diffusion (S65T) in tobacco leaf cells with both excitation alternatives at power levels $P_{diff}$. *Black curves*: 1PE; *gray curves*: 2PE. *Dotted curves*: Results for deeper cell layers. The curves are scaled to $G(0) \times F$ for the same average fluorescence $F$ to represent $\eta$ levels. Almost no correlated signal is left for 1PE. *Right*: Cellular autofluorescence in the same cell type. Less correlation can be seen for 1PE, indicating that the background is mainly due to scattering and/or weakly diffusing particles.

**TABLE 3 Achievable fluorescence detection rates per molecule $\eta(P_{diff})$ for EGFP in turbid tissue: $\eta$ obtained in surface and deeper layers of tobacco leaf epidermial cells for the photobleaching power threshold $P_{diff}$**

| | Surface cells 1PE | Surface cells 2PE | Deep cells 1PE | Deep cells 2PE |
|---|---|---|---|---|
| Control limit $P_{diff}$ | 15 $\mu$W | 7.5 mW | n.d. | 7.5 mW |
| $\eta$ (kcps/molecule) in cells at $P_{diff}$ | 0.75 ± 0.2 | 1.3 ± 0.3 | <0.2 | 1.1 ± 0.3 |
| $\eta$ (kcps/molecule) in solution at $P_{diff}$ | 1.5 ± 0.1 | 1.5 ± 0.2 | 1.5 ± 0.1 | 1.5 ± 0.2 |

even in the surface cell layers. Deeper cell layers (more than three) no longer gave usefully measurable FCS curves in 1PE, while almost no difference in signal quality could be observed in the two-photon case. The diffusion coefficient of GFP in the cytosol of these cells showed no difference from buffer solution, with a value around $D_{GFP} = 5(\pm 2) \times 10^{-7}$ cm$^2$/s, indicating that the viscosity of this plant cytosol is water-like. Table 3 summarizes the measured values of $\eta$ in tobacco leaf epidermal tissue and compares them with values in solution under the same power conditions.

### *Autofluorescence and scattering*

Autofluorescence of mammalian and plant cells is often considered to be one of the major problems encountered in ultrasensitive fluorescence applications such as FCS, especially in 1PE at wavelength ranges below 500 nm. Known intrinsic biological autofluorescent molecules include NADH, flavins such as FAD, FMN and flavoproteins, collagen, elastin, and lipofusion. Most plant cells also contain chlorophyll that is excited and fluoresces even at long wavelengths greater than 600 nm. Careful studies of cellular autofluorescence are therefore required for every FCS application, to determine the optimal fluorescent probe concentration level that best discriminates against autofluorescent background but still allows reliable fluctuation analysis. An upper limit of probe concentration for FCS measurements is usually micromolar, on the order of 1000 molecules in the measurement volume (Thompson, 1991). On the other hand, the concentration of the investigated dye system should be considerably higher than the detected concentration of autofluorescent particles $C_B$ that themselves show contributions to the correlation curve.

Autofluorescence studies were carried out in mammalian cells (RBL, HeLa, EMT6) and plant (tobacco leaf) cells; these are summarized in Table 4. For mammalian cells, we found that after the rapid decrease of an initial autofluorescence signal within seconds, which we associate with bleaching of immobile molecules, the background level remains steady. Intracellular measurements show a correlated background; however, hardly any additional correlation was observed at the cell surfaces. The measured intracellular correlation curves can be described by 3D particle diffusion with typically more than one diffusing species, which is similar to the findings of Brock et al. (1998). The average diffusion coefficients are $D_B \approx 10^{-7}$ cm$^2$/s, with values only slightly dependent on the measurement position in the cell. As expected, $F_B$ for 1PE is strongly dependent on the pinhole size, where the 25-$\mu$m case again corresponds to a two-photon background. At comparable $F_B$ for 2PE, the correlation amplitudes and thus $\eta_B$ are much lower, which can be explained if different molecules with low excitation cross sections or quantum yields but higher concentrations are present as autofluorescence sources. While the cell surface background $F_B$ is 1.5–2-fold higher than for the cell interior with 1PE at 488 and 543 nm, no significant difference can be observed for 850 and 920 nm. The overall background at 488 nm is a factor of 2 higher than at 543 nm. In contrast to the observed mammalian cells, background autocorrelation curves in plant cells are measurable only by 2PE, although the $F_B$ values are much lower, because the scattering at cell walls is avoided (Fig. 8, *right*). Table 4 summarizes $F_B$, $C_B$, $D_B$, and $\eta_B$ in all of our applications for the threshold powers $P_{diff}$.

Finally, autofluorescence spectra were taken in the focal measurement volume in RBL and plant cells for excitation

**TABLE 4 Properties of cellular autofluorescence in FCS applications**

| | Mammalian cells (RBL/CHO/HeLa) | | Plant cells (tobacco) | |
|---|---|---|---|---|
| | 1PE (543 nm) | 2PE (850 nm) | 1PE (488 nm) | 2PE (920 nm) |
| $F_B$ ($P_{diff}$) intracellular (kcps) | 2.5 | 2 | 11 | 1 |
| $D_B$ (cm$^2$/s) | $\sim 10^{-7}$ | (−)* | (−) | $\sim 10^{-9}$ |
| $\eta_B$ (kcps/molecule) | 0.75 | (−) | (−) | |
| $C_B$ (nM) | ~1 | (−) | (−) | |
| $F_B$ ($P_{diff}$) on membranes (kcps) | 1.2 | 0.8 | n.d. | n.d. |
| Required concentrations of TMR (nM) | 1–100 | 10–100 | n.d. | n.d. |
| Required concentrations of GFP (nM) | 10–100** | 10–100 | 1–100 | 1–100 |
| Visible cell damage threshold $P_{dam}$ (mW) | | 30 | | 38 |

*Autofluorescence background does not correlate.
**At 488 nm.

at 488 nm and at 850 nm (pulsed excitation) to compare one- and two-photon-induced backgrounds (Fig. 9). The autofluorescence spectra excited at 920 nm (not shown) are almost identical to those at 850 nm. The 2PE spectra are slightly blue-shifted compared to 1PE, which is most evident for the minimum in the emission near 620 nm in plant cells. An interesting observation is the spectral change in RBL cells when $P_{dam}$ is approached: a second maximum at 600 nm arises that is due to the induced autofluorescence. However, the FCS measurements of autofluorescence were performed at low power levels where the peak around 550 nm dominates, which is likely to be the long wavelength tail of flavins or flavoproteins.

## SUMMARY

Our measurements clearly show that FCS within living cells and on membranes is readily feasible with both 1PE and 2PE, although S/N values may be considerably smaller than in ideal aqueous solution because of autofluorescence and scattering background and the signal loss. With efficient photostable dyes such as rhodamine derivatives and GFP mutants, dynamics of molecules at nM concentrations (and thereby single molecules per sample volume) can easily be investigated. The dynamic range of observable diffusion mobilities is extended from $10^{-6}$ cm$^2$/s to $10^{-10}$ cm$^2$/s, opening up larger time windows for the observation of intramolecular dynamics of single molecules.

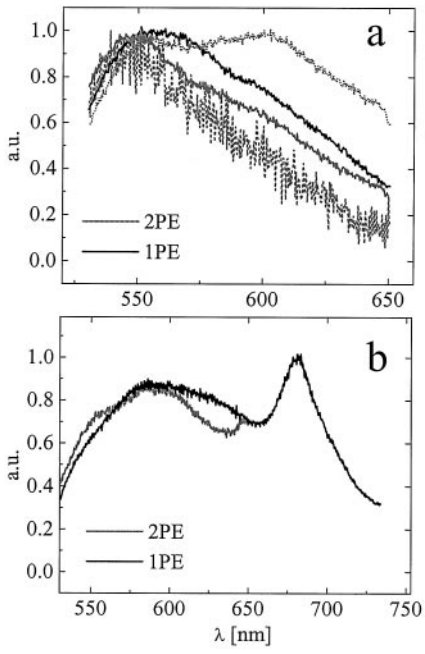


FIGURE 9 Autofluorescence spectra for 1PE at 488 nm (*black*) and 2PE at 850 nm (*gray*) in RBL (*a*) and tobacco leaf cells (*b*), as observed with long-pass (respectively short-pass) filters as described. The induced fluorescence effect of photodamage to RBL by 2PE at high power can be verified by comparing the RBL spectra for different illumination powers. *Gray dashed curve*, low powers $< P_{diff}$; *solid curve*, at $\sim P_{diff}$; *dotted curve*, at $P_{dam}$. The 2PE emission spectrum of tobacco in *b* is blue-shifted with respect to the 1PE spectrum.

The expected advantages of 2PE in terms of inherent depth discrimination, reduced photobleaching, and better penetration depth properties were confirmed. The useable $\eta$ values determined in solution for 1PE are equal to 2PE for the case of equal high-resolution volume sizes and in solution two to three times larger for the lower resolution focal volumes obtained by opening the confocal aperture in 1PE to optimize $\eta$. This situation changes in cells, especially for cells with thick walls such as plant cells, where effects of noncorrelating background like scattering of fluorescence signal are quite severe. Below power thresholds $P_{diff}$ for photobleaching artifacts, 2PE yields higher count rates per molecule $\eta$ and allows longer averaging with higher total illumination doses without fluorophore depletion in the confined cell volumes. Unlike solution applications, big confocal pinholes for 1PE do not improve $\eta$ in cells because the nonspecific background is much higher. However, with comparable effective sampling volumes for 2PE and 1PE (obtained with small detection apertures), count rates $F_B$ of autofluorescence background are similar. The stability of autofluorescent molecules, described as $\eta_B$, is often lower for 2PE. Furthermore, visible cell damage by the stationary 2PE beam seems to occur at lower relative powers than with 1PE, leaving much less headroom for a power increase above $P_{diff}$, the maximum power for artifact-free FCS.

The advantages of 2PE are the remarkably low accumulative photobleaching of the dye and the possibility of accessing deeper cell layers, combined with a very high axial resolution. Avoiding excitation along the illumination cone allows better handling of the focal spot without exposing the whole depth of the cell or tissue. In single layers of mammalian cells, if the concentration control is not crucial, the two excitation alternatives are equally good and yield the same FCS measurement results. Intracellular S/N values for 2PE are slightly higher; on the other hand, one-photon experiments are easier to perform, so that 2PE may not be justified here. However, for all applications where scattering is present, like plant cells or deeper tissue layers, two-photon FCS is highly recommended.

Most autofluorescence problems encountered in applying FCS in living preparations can be overcome by careful studies of the biological preparation of interest and selection of proper fluorophores in advance of the measurements. The fluorescence signal $F$ should be kept considerably (5–10 times) higher than the expected background signal $F_B$ during the whole measurement, which can be achieved by choosing dyes with high count rates per molecule $\eta$ and/or by applying high labeling densities. However, large fluorophore concentrations more than micromolar are not efficient in FCS, because $G(0) \propto \langle N \rangle^{-1}$ eventually becomes too small for fluctuation analysis. If $F_B > 0.1F$, correlations of any background fluorescence with high $\eta_B$ have to be taken into account as an additional contribution to the correlation curve Eq. 4. Fortunately it has turned out that autofluorescence has not seriously inhibited FCS in the experiments in

living cells and tissues reported here and in a variety of unpublished experiments ongoing in our laboratories.

## APPENDIX: GEOMETRICAL CONSIDERATIONS AND EFFECTIVE MEASUREMENT VOLUMES $V_{eff}$

It has been shown (Elson and Magde, 1974; Aragón and Pecora, 1976) that the correlation curve of Eq. 1 may be calculated analytically for several simple cases of number fluctuations if the optical convolution factors in Eqs. 2 and 3, $S(\underline{r})*\Omega(\underline{r})$ for 1PE and $S^2(\underline{r})*\Omega(\underline{r})$ with $\Omega(\underline{r}) = 1$ for 2PE, can be approximated as Gaussian distributions in radial and axial dimensions. For this case, the volume integrals are finite, and the amplitude $G(0)$ of the correlation function Eq. 1 can be written as $G(0) = V_{eff}^{-1}\langle C\rangle^{-1}$ with an effective detection volume (Mertz et al., 1995; Schwille et al., 1997b).

For the intensity distribution $S(\underline{r})$ in three dimensions, the Gaussian approximation is not strictly valid. With underfilled back aperture, the axial distribution is Lorentzian rather than Gaussian, while the diffraction-limited case for overfilled back aperture and the calculation for $\Omega(\underline{r}) \neq 1$ with confocal pinholes in 1PE require numerical computation (Sandison et al., 1994, 1995; Xu and Webb, 1997). Such calculations of the effects of finite aperture sizes in FCS are in progress (Hess et al., unpublished observations). However, to a first approximation, a 3D Gaussian assumption for $\Omega(r)$ and $S(\underline{r})$ can often be experimentally justified for both excitations by good results in fitting calibration data. As pointed out by previous investigators applying two-photon FCS (Berland et al., 1995), the Gaussian evaluation may not simultaneously reveal consistent absolute values for the independent experimental parameters.

For 2PE with $\Omega(\underline{r}) = 1$, Mertz et al. (1995) showed that the effective focal volume $V_{eff}$ is generally described in even moments of the excitation intensity $S(\underline{r})$ as

$$V_{\mathrm{eff,2PE}} = \left[\int_V S^2(\underline{r})\mathrm{d}V\right]^2 \Big/ \int_V S^4(\underline{r})\mathrm{d}V = \gamma^{-1}\int_V S^2(\underline{r})\mathrm{d}V,$$

where $\gamma$ is the inherent volume contrast. With an ellipsoidal 3D Gaussian for the intensity profile $S(\underline{r})$, $\gamma = \sqrt{2}/4 = 0.35$, while for the diffraction-limited volume $\gamma = 0.26$, as calculated by Xu and Webb (1997), indicating a 35% discrepancy in the Gaussian approximation. Without a pinhole, $V_{eff}$ is, in principle, fully defined by the numerical aperture and the excitation wave-length $\lambda_e$. If $S(\underline{r})$ is assumed to be Gaussian with $1/e^2$ values $r_{s,0}$ and $z_{s,0}$, the effective volume size is $V_{\mathrm{eff,2PE}} = (\pi/2)^{3/2} r_{s,0}^2 z_{s,0}$.

To simultaneously treat 1PE and 2PE, we approximate the convolution factor in 1PE as a squared Gaussian, $S(\underline{r})*\Omega(\underline{r}) \equiv W^2(\underline{r})$, which is, in the case of an infinitesimally small critical pinhole, except for wavelength factors consistent with 2PE, where the convolution is just the square $S^2(\underline{r})$ of the illumination function:

$$W^2(\underline{r}) = \exp(-2ar^2/r_{s,0}^2)\exp(-2bz^2/z_{s,0}^2)$$

$$\equiv \exp(-4r^2/r_{w,0}^2)\exp(-4z^2/z_{w,0}^2).$$

The exponential factors $a$ and $b$ are introduced by the collection function $\Omega(\underline{r})$ and depend on pinhole size. For wide-field detection without any pinhole, $\Omega(\underline{r}) = 1$ and $a = b = 1$. This form applies in theory only to cylindrical illumination by a Gaussian beam, where $z_{s,0} \rightarrow \infty$ and the axial restriction has to be introduced by the sample. For critical confocal pinholes, $a = b = 2$ and $r_{w,0}, z_{w,0} = r_{s,0}, z_{s,0}$. An effective volume element can be defined analogously to the 2PE case, where now $V_{\mathrm{eff,1PE}} = (\pi/2)^{3/2} r_{w,0}^2 z_{w,0}$. The 1PE parameters $r_{w,0}$ and $z_{w,0}$ are dependent on both the illumination and detection optics, because $S(\underline{r})$ scales with excitation wavelength $\lambda_e$ and $\Omega(\underline{r})$ with emission wavelength $\lambda_f$. For both 1PE and 2PE, $V_{eff}$ and the $1/e^2$ values of given $S(\underline{r})$ and $W(\underline{r})$ can be estimated experimentally by calibration of the system with a dye of known dynamic properties, as explained. For the sake of simplicity, the abbreviations $r_0$ and $z0_0$ are used throughout the text for $r_{s,0}$ and $z_{s,0}$ in the 2PE case and for $r_{w,0}$ and $z_{w,0}$ in the 1PE case.

We thank Paul S. Pyenta, Department of Chemistry and Chemical Biology, for providing the EGFP-expressing RBL cells; Dr. Rainer H. Köhler, Plant Sciences, for the supply of tobacco plants and assistance in the test experiments with and without GFP; and Jonas Korlach, Dr. Rebecca Williams, and Prof. Barbara Baird for critical reading of the manuscript.

The work was financed by National Institutes of Health grant P412 RR04224 and National Science Foundation grant B1R 8800278. PS received a Feodor-Lynen fellowship from the Alexander von Humboldt Foundation and support from EVOTEC BioSystems GmbH, Hamburg.

## REFERENCES

Aragón, S. R., and R. Pecora. 1976. Fluorescence correlation spectroscopy as a probe of molecular dynamics. *J. Chem. Phys.* 64:1791–1803.

Berland, K. M., P. T. C. So, and E. Gratton. 1995. Two-photon fluorescence correlation spectroscopy—method and application to the cellular environment. *Biophys. J.* 68:694–701.

Bieschke, J., and P. Schwille. 1997. Aggregation of prion protein investigated by dual-color fluorescence cross-correlation spectroscopy. *In* Fluorescent Microscopy and Fluorescent Probes, Vol. 2. J. Slavik, editor. Plenum Press, New York. 81–86.

Bonnet, G., O. Krichevsky, and A. Libchaber. 1998. Kinetics of conformational fluctuations in DNA hairpin-loops. *Proc. Natl. Acad. Sci. USA.* 95:8602–8606.

Brand, L., C. Eggeling, C. Zander, K. H. Drexhage, and C. A. M. Seidel. 1997. Single-molecule identification of Coumarin-120 by time-resolved fluorescence detection: comparison of one- and two-photon excitation in solution. *J. Phys. Chem. A.* 101:4313–4321.

Brock, R., M. Hink, and T. Jovin. 1998. Fluorescence correlation microscopy of cells in the presence of autofluorescence. *Biophys. J.* 75: 2547–2557.

Denk, W., J. H. Strickler, and W. W. Webb. 1990. Two-photon laser scanning fluorescence microscopy. *Science.* 248:73–76.

Eigen, M., and R. Rigler. 1994. Sorting single molecules: applications to diagnostics and evolutionary biotechnology. *Proc. Natl. Acad. Sci. USA.* 91:5740–5747.

Elson, E. L., and D. Magde. 1974. Fluorescence correlation spectroscopy. I. Conceptual basis and theory. *Biopolymers.* 13:1–27.

Feder, T. J., I. Brust-Mascher, J. P. Slattery, B. Baird, and W. W. Webb. 1996. Constrained diffusion or immobile fraction on cell surfaces: a new interpretation. *Biophys. J.* 70:2767–2773.

Ghosh, R. N., and W. W. Webb 1994. Automated detection and tracking of individual and clustered cell surface low density lipoprotein receptor molecules. *Biophys. J.* 66:1301–1318.

Haugland, R., editor. 1996. Handbook of Fluorescent Probes and Research Chemicals, 6th Ed. Molecular Probes, Eugene, OR.

Haupts, U., S. Maiti, P. Schwille, and W. W. Webb. 1998. Dynamics of fluorescence fluctuations in green fluorescent protein observed by fluorescence correlation spectroscopy. *Proc. Natl. Acad. Sci. USA.* 95: 13573–13578.

Huang, Z. P., and N. L. Thompson. 1996. Imaging fluorescence correlation spectroscopy: nonuniform IgE distributions on planar membranes. *Biophys. J.* 70:2001–2007.

Kask, P., R. Günther, and P. Axhausen. 1997. Statistical accuracy in fluorescence fluctuation experiments. *Eur. Biophys. J.* 25:163–169.

Kettling, U., A. Koltermann, P. Schwille, and M. Eigen. 1998. Real time enzyme kinetics of restriction endonuclease *Eco*RI monitored by dual-color fluorescence cross-correlation spectroscopy. *Proc. Natl. Acad. Sci. USA.* 95:14116–1420.

Kinjo, M., and R. Rigler. 1995. Ultrasensitive hybridization analysis using fluorescence correlation spectroscopy. *Nucleic Acids Res.* 23: 1795–1799.

Köhler, R. H., J. Cao, W. R. Zipfel, W. W. Webb, and M. Hanson. 1997. Exchange of protein molecules through connections between higher plant plastids. *Science.* 276:2039–2042.

Koltermann, A., U. Kettling, J. Bieschke, T. Winkler, and M. Eigen. 1998. Rapid assay processing by integration of dual-color fluorescence cross-correlation spectroscopy: high throughput screening for enzyme activity. *Proc. Natl. Acad. Sci. USA.* 95:1421–1426.

Koppel, D. E. 1974. Statistical accuracy in fluorescence correlation spectroscopy. *Phys. Rev. A.* 10:1938–1945.

Koppel, D. E., D. Axelrod, J. Schlessinger, E. L. Elson, and W. W. Webb. 1976. Dynamics of fluorescence marker concentration as a probe of mobility. *Biophys. J.* 16:1315–1329.

Koppel, D. E., F. Morgan, A. E. Cowan, and J. H. Carson. 1994. Scanning concentration correlation spectroscopy using the confocal laser microscope. *Biophys. J.* 66:502–507.

Magde, D., E. L. Elson, and W. W. Webb. 1972. Thermodynamic fluctuations in a reacting system—measurement by fluorescence correlation spectrocsopy. *Phys. Rev. Lett.* 29:705–708.

Magde, D., E. L. Elson, and W. W. Webb. 1974. Fluorescence correlation spectroscopy. II. An experimental realization. *Biopolymers.* 13:29–61.

Magde, D., E. L. Elson, and W. W. Webb. 1978. Fluorescence correlation spectroscopy. III. Uniform translation and laminar flow. *Biopolymers.* 17:361–376.

Maiti, S., U. Haupts, and W. W. Webb. 1997. Fluorescence correlation spectroscopy: diagnostics for sparse molecules. *Proc. Natl. Acad. Sci. USA.* 94:11753–11757.

Menon, A. K., D. Holowka, W. W. Webb, and B. Baird. 1986. Clustering, mobility, and triggering activity of small oligomers of immunoglobulin E on rat basophilic leukemia cells. *J. Cell Biol.* 102:534–540.

Mertz, J., C. Xu, and W. W. Webb. 1995. Single-molecule detection by two-photon-excited fluorescence. *Opt. Lett.* 20:2532–2534.

Mets, Ü., and R. Rigler. 1994. Submillisecond detection of single rhodamine molecules in water. *J. Fluoresc.* 4:259–264.

Palmer, A. G., and N. Thompson. 1987. Molecular aggregation characterized by high order autocorrelation in fluorescence correlation spectroscopy. *Biophys. J.* 52:257–270.

Petersen, N. O. 1986. Scanning fluorescence correlation spectroscopy. I. Theory and simulation of aggregation measurements. *Biophys. J.* 49: 809–815.

Petersen, N. O., P. L. Hoddelius, P. W. Wiseman, O. Seger, and K. E. Magnusson. 1993. Quantitation of membrane-receptor distributions by image correlation spectroscopy—concept and application. *Biophys. J.* 65:1135–1146.

Politz, J. C., E. S. Browne, D. E. Wolf, and T. Pederson. 1998. Intranuclear diffusion and hybridization state of oligonucleotides measured by fluorescence correlation spectroscopy in living cells. *Proc. Natl. Acad. Sci. USA.* 95:6043–6048.

Qian, H. 1990. On the statistics of fluorescence correlation spectroscopy. *Biophys. Chem.* 38:49–57.

Qian, H., and E. L. Elson. 1991. Analysis of confocal laser-microscope optics for 3-D fluorescence correlation spectroscopy. *Appl. Opt.* 30: 1185–1195.

Rauer, B., E. Neumann, J. Widengren, and R. Rigler. 1996. Fluoresence correlation spectrometry of the interaction kinetics of tetramethylrhodamin $\alpha$-bungarotoxin with *Torpedo californica* acetylcholine receptor. *Biophys. Chem.* 58:3–12.

Rigler, R., Ü. Mets, J. Widengren, and P. Kask. 1993. Fluorescence correlation spectroscopy with high count rates and low background: analysis of translational diffusion. *Eur. Biophys. J.* 22:169–175.

Rigler, R., and J. Widengren. 1990. Ultrasensitive detection of single molecules by fluorescence correlation spectroscopy. *Bioscience.* 3:180–183.

Sanchez, E. J., L. Novotny, G. R. Holtom, and X. S. Xie. 1997. Room-temperature fluorescence imaging and spectroscopy of single molecules by two-photon excitation. *J. Phys. Chem. A.* 101:7019–7023.

Sandison, D. R., D. W. Piston, R. M. Williams, and W. W. Webb. 1995. Quantitative comparison of background rejection, signal-to-noise-ratio, and resolution in confocal and full-field laser-scanning-microscopes. *Appl. Opt.* 34:3576–3588.

Sandison, D. R., and W. W. Webb. 1994. Background rejection and signal-to-noise optimization in confocal and alternative fluorescence microscopes. *Appl. Opt.* 33:603–615.

Schwille, P., J. Bieschke, and F. Oehlenschläger. 1997a. Kinetic investigations by fluorescence correlation spectroscopy: the analytical and diagnostic potential of diffusion studies. *Biophys. Chem.* 66:211–228.

Schwille, P., J. Korlach, and W. W. Webb. 1999. Fluorescence correlation spectroscopy with single molecule sensitivity on cell and model membranes. *Cytometry.* 36:176–182.

Schwille, P., F.-J. Meyer-Almes, and R. Rigler. 1997b. Dual-color fluorescence cross-correlation spectroscopy for multicomponent diffusional analysis in solution. *Biophys. J.* 72:1878–1886.

Schwille, P., F. Oehlenschläger, and N. Walter. 1996. Quantitative hybridization kinetics of DNA probes to RNA in solution followed by diffusional fluorescence correlation analysis. *Biochemistry.* 35:10182–10193.

Sheppard, C. J. R., and H. J. Matthews. 1987. Imaging in high-aperture optical systems. *J. Opt. Soc. Am. A.* 4:1354–1360.

Swaminathan, R., C. P. Hoang, and A. S. Verkman. 1997. Photobleaching recovery and anisotropy decay of green fluorescent protein S65T in solution and cells: cytoplasmic viscosity probed by GFP translational and rotational diffusion. *Biophys. J.* 72:1900–1907.

Thompson, N. L. 1991. Fluorescence correlation spectroscopy. *In* Topics in Fluorescence Spectroscopy, Vol. 1. J. R. Lakowicz, editor. Plenum Press, New York. 337–378.

Tsien, R. Y. 1998. The green fluorescent protein. *Annu. Rev. Biochem.* 67:509–544.

Widengren, J., Ü. Mets, and R. Rigler. 1995. Fluorescence correlation spectroscopy of triplet states in solution: a theoretical and experimental study. *J. Chem. Phys.* 99:13368–13379.

Widengren, J., and R. Rigler. 1996. Mechanisms of photobleaching investigated by fluorescence correlation spectroscopy. *Bioimaging.* 4:149–157.

Williams, R. M., D. Piston, and W. W. Webb. 1994. Two-photon molecular excitation provides intrinsic 3-dimensional resolution for laser-based microscopy and microphotochemistry. *FASEB J.* 8:804–813.

Xu, C., and W. W. Webb. 1997. Multiphoton excitation of molecular fluorophores and nonlinear laser microscopy. *In* Topics in Fluorescence Spectroscopy 5. J. Lakowicz, editor. Plenum Press, New York.

Xu, C., W. Zipfel, J. B. Shear, R. M. Williams, and W. W. Webb. 1996. Multiphoton fluorescence excitation: new spectral windows for biological nonlinear microscopy. *Proc. Natl. Acad. Sci. USA.* 93:10763–10768.